Structural Eng./Earthquake Eng., JSCE, Vol. 21, No. 1, 11s—26s, 2004 January
(J. Struct. Mech. Earthquake Eng., JSCE, No. 752/ I —66)

EXPERIMENTAL STUDY OF REINFORCED CONCRETE BRIDGE PIERS SUBJECTED TO BI-DIRECTIONAL QUASI-STATIC LOADING

Kazuhiro TSUNO[1] and Robert PARK[2]

[1]Member of JSCE, Master Eng, First Design Division, First Construction Department, Kanagawa Construction Bureau, Metropolitan Expressway Public Corp.
(1-2-4 Shinkoyasu, Kanagawa-ku, Yokohama, Kanagawa 221-0013, Japan)
[2]Phd. Eng, Emeritus Professor, Dept of Civil Eng, University of Canterbury
(Private Bag 4800, Christchurch, New Zealand)

This research aims to determine the effect of loading pattern on the damage of a reinforced concrete bridge column. Five specimens were tested with uni-directional or bi-directional cyclic loading patterns combined with a uniform axial load. From the test results, the theoretical plastic hinge zone length was calculated considering the yield penetration effect and the energy dissipated by the specimens was obtained.

Key Words: *bi-directional cyclic loading, RC column members, plastic hinge zone length, energy dissipation*

1. INTRODUCTION

For the development of the performance-based design method for a bridge column, how to predict the performance of the column is an important task needing to be studied. The needed studies include how to predict the capacity of a column for displacement or energy dissipation and how to estimate the damage accumulation on the column during a major earthquake. The analytical damage estimation is a useful and effective tool not only for the performance-based design method but also for the estimation of residual energy capacity and retrofitting necessary for the damaged columns after a major earthquake. The problem here is that the ductile behaviour of a reinforced concrete column has been reported as affected by the loading pattern used in the test.

Kawashima & Koyama [1], Ozaka et al. [2], Takemura & Kawashima [3] and Hoshikuma et al.[4] reported the effect of different cyclical loading pattern in one lateral direction on reinforced concrete bridge columns. They found that the greater the number of loading cycles to the same displacement, the smaller the maximum displacement of the column before its ultimate state was reached. The maximum lateral strength of the column reached, however, was not significantly affected by the loading pattern used in the tests. Concerning bi-directional loadings, Miyaji et al.[5], Sato et al.[6] and Mashiko et al.[7] revealed that there was an interaction effect between the lateral strength in two directions, perpendicular to each other of a reinforced concrete column, and the lateral strength in one direction decreased when the deflection of the column in a direction perpendicular to the measured strength was significant. The information concerning the effect of different loading patterns, however, is still limited and the damage accumulation of reinforced concrete column, in different loading patterns has not clearly understood, yet.

The aims of this research effort are to analyse the effect of the loading pattern on a reinforced concrete column that is seismically detailed and to develop a procedure to estimate the damage and the failure of the column caused by a seismic loading. In the tests for this research, some different loading patterns, including bi-directional loading patterns, based on a loading pattern which is regarded as the standard in New Zealand and different from that commonly used

in Japan are applied to the specimens seismically detailed using the Japanese specification.

This is the first report of the research. In this report, the test procedure and the results are shown, and the theoretical plastic hinge zone length and the dissipated energy are calculated from the results and discussed.

2. TEST PROGRAM

(1) Testing procedure

a) Test set-up

The test specimens were supported between two universal joints at the top of the column and the bottom of the base block, and axially loaded by a DARTEC universal testing machine. A hydraulic jack placed between the column and a loading rig applied a lateral load to the loading rig had a counter weight. The DARTEC machine was controlled by a computer and automatically maintained a uniform axial load on the specimen. The base block of the specimen was heavily reinforced so as not to be affected by the lateral force applied by fixing bolts and base plates of the loading rig and the counter weight basket as a rigid body. One set of loading rig with counter-weight basket was used for the specimens-1, 2 and 5 in the east-west direction, and two sets were used for specimens-3 and 4 in east-west and north-south directions in order to apply bi-directional horizontal load. **Fig.1** and **Fig.2** show the test set-up.

b) Loading patterns

Originally, five identical test specimens were planned to be tested with five different loading patterns. However, the strength of the concrete cast in one column was found to be less than half of the design strength due to an error in manufacturing the concrete, as seen in §3.(1). Therefore, the original plan was revised to test four identical test specimens, Specimen-1 to 4, with four different loading patterns and one weak-concrete column, Specimen-5, with the standard loading pattern which was also used for Specimen-1.

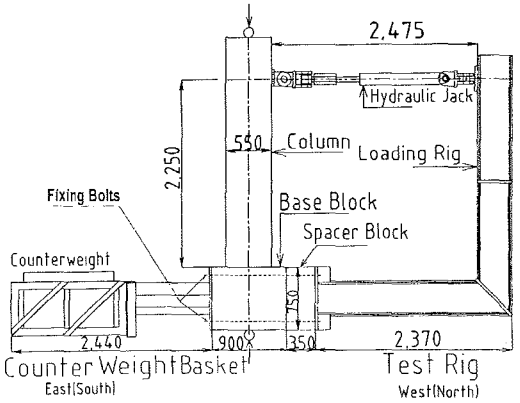

Fig.1 Test Set-Up [unit: mm]

Specimen-1

Specimen-1 was loaded by the standard loading pattern used at the University of Canterbury (Park [9]) seen in **Fig.3** as a bench mark test. This loading pattern is supposed to test well the fatigue of reinforcing bars and the damage at the concrete of the column and has been widely used in New Zealand.

The test is started by applying the lateral load to the specimen in one direction, and the load is increased until it reaches the calculated or measured first yielding load of the specimen or three quarters of the calculated ideal strength of the specimen, whichever is less. Then the specimen is loaded in the opposite direction using the same procedure. The largest displacement point achieved in the first cycle defines the secant stiffness of the specimen on the load-displacement relationship for each direction. Then the average of the displacements corresponding to the intersection points of the straight lines for the secant stiffness and the horizontal lines for the ideal strength of the specimen is defined as the reference yielding displacement δ_y as seen in **Fig.4**.

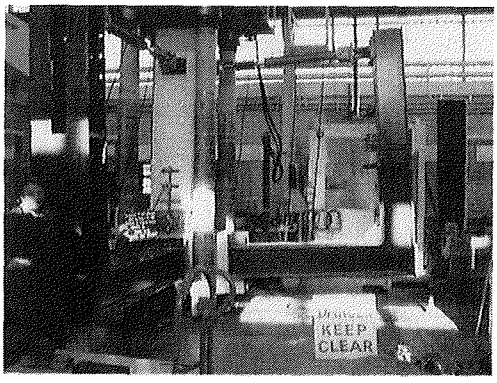

Fig.2 Test Set-Up (Two Sets of Rigs with Specimens-3)

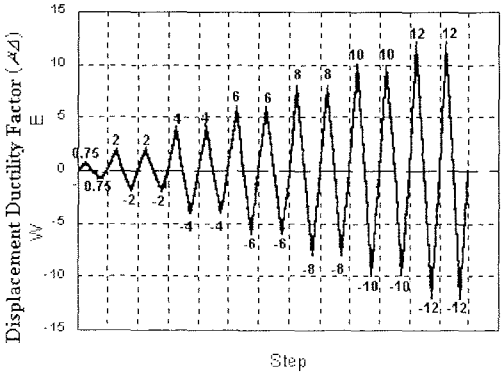

Fig.3 Loading Pattern for Specimen-1

This procedure to determine δ_y is used for all other specimens, too. For the second load cycle, the test is controlled by displacement of the specimen at the loading point. The maximum imposed displacement for the next two cycles is twice of δ_y, and then the maximum displacement is increased by $2\delta_y$ steps after every two cycles with the same displacement, namely two cycles for μ_Δ=2, two cycles for μ_Δ=4, two cycles for μ_Δ=6, etc. Here, the displacement ductility factor μ_Δ is

$$\mu_\Delta = \delta_{max} / \delta_y \qquad (1)$$

Where, δ_{max} is the maximum imposed displacement in a loading cycle. The test specimen was considered to have failed when the lateral strength of the column was smaller than 80% of the maximum lateral load measured during the first cycle to $\pm 2\delta_y$. This definition of the ultimate state of a specimen was applied to also Specimens-3, 4 and 5. For all the rest of this research report, "ultimate state" means that defined by Zahn et al. [10] as above.

Specimen-2

Fig.5 shows the loading pattern used for Specimen-2 which was completely opposite to that used for Specimen-1, except for the first cycle to three-quarters of the ideal strength used to determine the reference yield displacement δ_y. The maximum displacement of the second and third cycle was $12\delta_y$, which was derived from the test result of Specimen-1, then the applied maximum displacement for a loading cycle was decreased by $2\delta_y$ in every two cycles. The test was terminated after two cycles of $2\delta_y$.

Specimen-3

A bi-directional loading was used for Specimen-3. The standard loading pattern, same as that for Specimen-1, was applied for each north-south and east-west direction in one direction at a time.

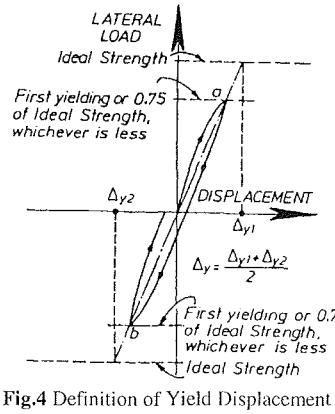

Fig.4 Definition of Yield Displacement (Park [9])

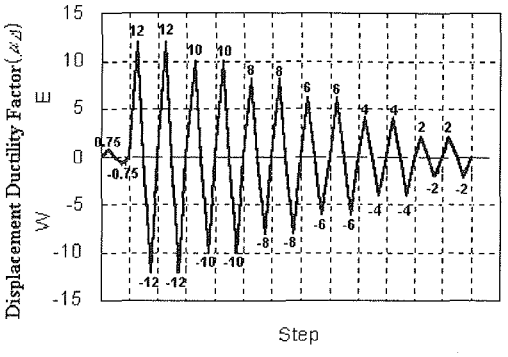

Fig.5 Loading Pattern for Specimen-2

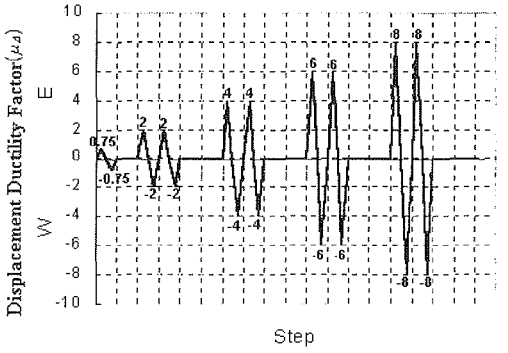

Fig.6(a) Loading pattern for Specimen-3: Loading cycle for East-West direction

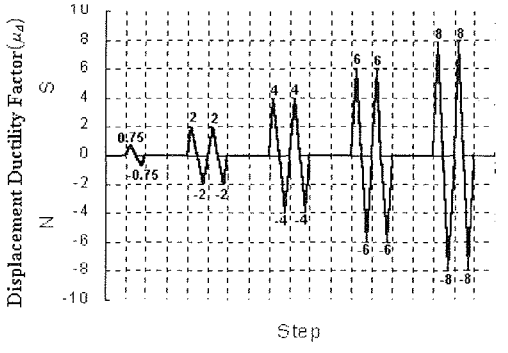

Fig.6(b) Loading pattern for Specimen-3: Loading cycle for North-South direction

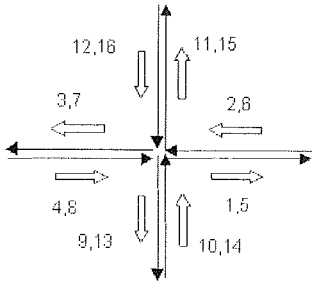

Fig.6(c) Loading pattern for Specimen-3: Loading orbit at the top of the specimen

After the reference yield displacement δ_y was determined, two cycles of $2\delta_y$ were applied in the east-west direction, and after the column was returned to the initial position (zero-displacement), the same two cycles were applied in the north-south direction, i.e. a total of four cycles of $2\delta_y$ were applied. Two cycles of $4\delta_y$ in the east-west and two cycles of $4\delta_y$ in the north-south direction followed subsequently, and the displacement amplitude for a loading cycle was increased by $2\delta_y$ in every four cycles.

Specimen-4

A bi-directional loading pattern was used. From the second loading cycles, the previous direction of loading was held at the maximum reached displacement while loading in the new direction was applied. The loading amplitude was increased by $2\delta_y$, in every one complete cycle.

Specimen-5

The same loading procedure as for Specimen-1 was used also for Specimen-5, in order to compare the result to that from Specimen-1 and analyse the effect of lower concrete strength.

(2) Design of specimens

The test specimens are models of a reinforced concrete bridge column with a square section, designed by the Japanese specification [6]. The prototype column is a design example in "Seismic Design Data for Highway Bridges" [11]. The original column cross section of the design example is 5m×2.2m, but this was modified to a 3m×3m square section to meet the same design condition with that for the prototype. The natural period might be different, but the possible strongest design lateral seismic coefficient was used as the prototype. It was then scaled down to the test specimen with 550mm×550mm section. The axial load applied to the specimen was determined so as to keep the same stress at the base of the column as that for the prototype.

The specimen shown in **Fig.8** is designed to follow the scale ratio equal to 5.45, which is the ratio 3m to 550mm, for as many details as possible, in order to avoid the scale effect in the experiment.

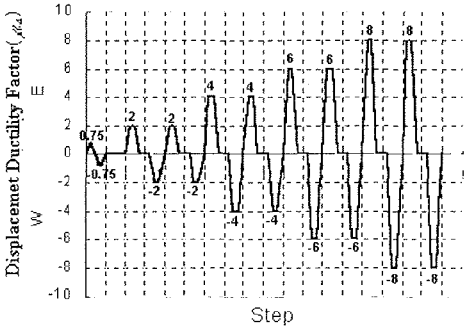

Fig.7(a) Loading pattern for Specimen-4: Loading pattern for East-West direction

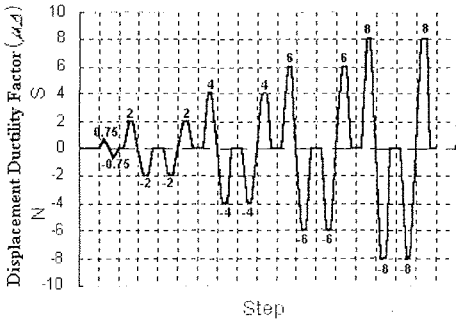

Fig.7(b) Loading pattern for Specimen-4: Loading pattern for North-South direction

(3) Measurement

Five potentiometers are mounted on each surface of the test specimen as seen in **Fig.9(a)** and **Fig.9(b)**. The curvature ϕ is calculated by Eq(2).

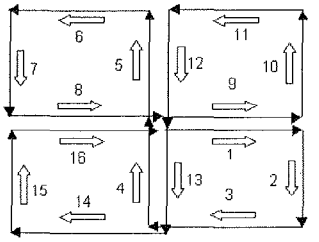

Fig.7(c) Loading pattern for Specimen-4: Loading orbit at the top of the specimen

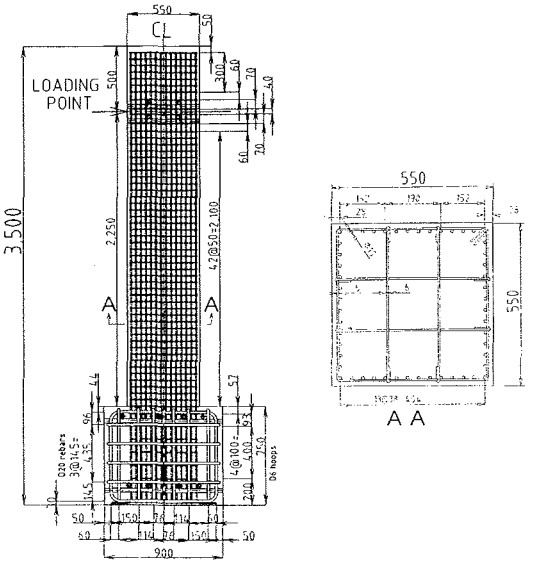

Fig.8 Reinforcement Arrangement of the Specimen [unit:mm]

Table 1 Specification of Specimens

		specimen	comments
Section		550*550mm	
Cover (from centre line of main-bar)		28mm	
Cover (pure)		11mm	
Height of loading point		2250mm	
Con-crete	Design strength	23.5 MPa	f'_{ck}
	Max size of aggregate	6mm	
Main-bars	Yield strength	300 MPa	
	Diameter	10mm	
	Sectional area	78.5 mm^2	one bar
	Total number	52	
	Steel ratio [a)]	1.174%	A_{st}/A_g
Trans-verse Bars	Yield strength	300 MPa	
	Diameter	6mm	
	Sectional area	28.3mm	A_h
	Vertical centre-to-centre spacing	50mm	s
	Effective length	190mm	d
	Steel ratio [a)]	1.035%	$A_h/(sd)$
Axial Load	Axial load	311 kN	N
	Stress	1.027 MPa	N/A_g
	Stress / Capacity	4.36%	$N/A_g f'_{ck}$

a) The yield strength of reinforcement is considered.

$$\phi = \frac{d_2 - d_1}{L_{pot} x_{pot}} \qquad (2)$$

Where, d_1 and d_2 are the contraction or expansion measured on the opposite sides at the same level; L_{pot} is the horizontal distance between the potentiometers mounted on the opposite sides; and x_{pot} is the vertical distance between two potentiometers mounted in the same face of the test specimen (e.g. 80, 150 or 200mm in **Fig.9(a)**) where d_1 or d_2 is measured. x_{pot} was decided from the size and number of potentiometers available. The positive values of measured d_1 or d_2 are supposed to include some extra length due to the yield penetration of the vertical main-bars. The absolute value of yield penetration itself is not measured, but it is eliminated based on some assumptions in the analysis in 4.(2). The locations of the strain-gauges are seen in **Fig.10**.

3. TEST

(1) Properties of materials

6mm and 10mm diameter deformed bars were used for the transverse reinforcement and the main vertical bars, respectively. The design strength was 300MPa for both types of reinforcing bars. **Table 2** shows the results of tensile tests of the bars. The average concrete compressive strength is shown in **Table 3**.

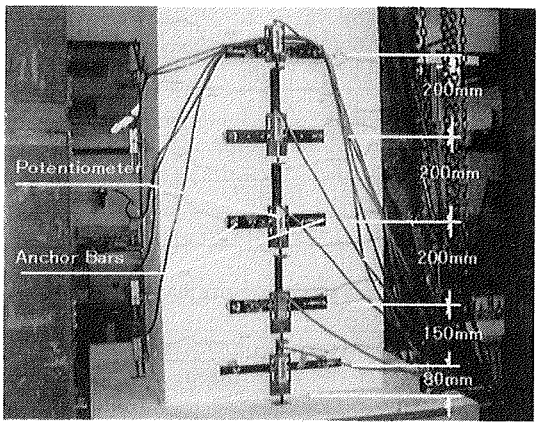

Fig.9(a) Location of Potentiometers for Curvature

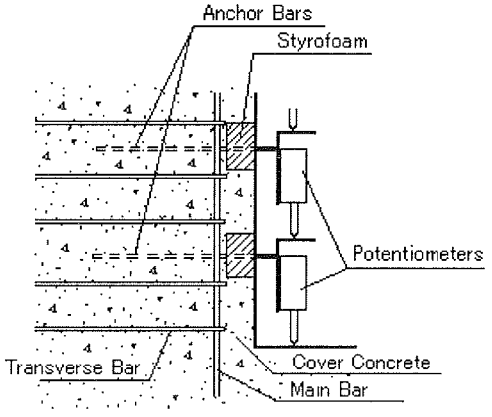

Fig.9(b) Setting Detail of Potentiometers for Curvature

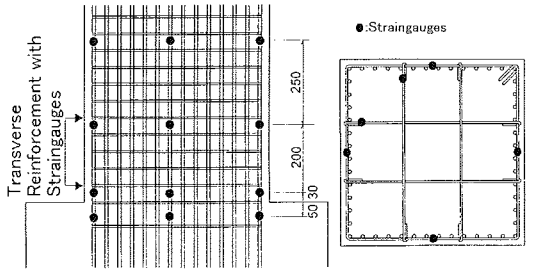

Fig.10 Location of Strain-Gauges [unit:mm]

In **Table 2**, f_y is the yield stress; E_s is the Modulus of Elasticity; f_{su} is peak stress; ε_{su} is the strain at peak stress; and ε_{sf} is the fracture strain. Each number is the average of results from three test samples. The 6mm bars did not have a yield plateau and were more brittle than the 10mm bars.

(2) Theoretical flexural strength of the column

a) Ideal flexural strength of the test specimens

The ideal flexural strength of the test specimens were calculated using the actual properties of the materials shown in §3.(1), in order to determine the

Table 2 Test Results of Reinforcing Bars

Re-bar size	6mm	10mm
f_y (MPa)	285.6	306.0
E_s (MPa)	212100	203400
f_{su} (MPa)	485.4	438.8
ε_{su}	0.0777	0.1920
ε_{sf}	0.0992	0.2994

Table 3 Average Concrete Compressive Strength on the Day of Test

Specimen No.	Average Compressive Strength (MPa)	
	Column	Base-bolock
1	30.7	19.6
2	30.7	19.6
3	27.0	29.4
4	29.4	29.4
5	10.9	*26.6

*28th day

reference yield displacement of each test specimen. The ideal flexural strength is calculated based on the following assumptions used in the NZ3101(1995) [12]. The maximum compressive strain of concrete is 0.003; the stress in the reinforcement is E_s times the steel strain except that the maximum and minimum stress is equal to $+f_y$ and $-f_y$ respectively; the tensile strength of the concrete is neglected; and the concrete compressive stress is represented by a rectangular distribution with the stress equal to $0.85f'_c$ and a length equal to 0.85c. E_s is Young's modulus of elasticity of the reinforcement; f'_c is the specified compressive strength of concrete; and c is the distance from the extreme compression fibre to the neutral axis.

Sato et al.[13] tested some reinforced concrete columns at the University of Canterbury using the same experimental procedure as that used for this project, and described the P-δ effect of the tests. From **Fig.11**, the P-δ effect due to the loading arrangement in this series of tests is calculated as follows.

$$\frac{\Delta'/\cos\theta}{\Delta} = \frac{a}{b\cos\theta} \qquad (3)$$

therefore,

$$\Delta' = \frac{a}{b}\Delta \qquad (4)$$

where, $a = 750 + 50 = 800$mm

$b = 3500 + 50 + 175 = 3725$mm

$$\therefore \quad P_e\Delta' = P_e\frac{800}{3725}\Delta = 0.215\Delta P_e \qquad (5)$$

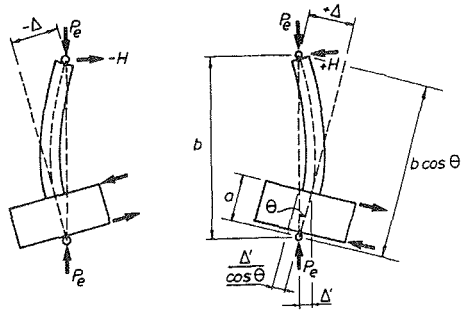

Fig.11 P-δ effect of the tests

Table 4 Ideal Flexural Strength M_n of Test Specimens

No. of specimen	M_n (kNm)	
	Without P-δ	With P-δ
1	382.6	381.8
2	382.6	381.8
3	378.8	378.0
4	381.3	380.5
5	343.9	343.1

The calculated values for the ideal flexural strength for the test specimens are shown in **Table 4**.

b) Moment-curvature analysis

The flexural strength of the test specimens were also estimated using the moment-curvature analysis method introduced by Mander et al. [14], for a comparison. The lateral load-displacement relationship for the specimen 1 and 2 calculated from the moment-curvature analysis is shown in **Fig.12**. **Table 5** shows the ideal lateral strength of the specimens at the loading point obtained by the moment-curvature analysis and NZ3101 [12] derived from **Table 4**.

(3) Observed features during the tests

a) Specimen-1

The test of Specimen-1 was terminated after the two cycles of $12\delta_y$ were completed. In the second cycle to $12\delta_y$, four main-bars were broken in tension. **Fig.13** shows the condition of Specimen-1 after the test.

b) Specimen-2

A maximum displacement $12\delta_y$ was applied in both east and west directions after the first cycle to the yield δ_y. When the displacement reached $+12\delta_y$, some cover concrete at the bottom on the east face had spalled off. When the displacement returned zero, the cover concrete buckled outwards over a relatively large area on the west face, at 200mm to 300mm above the base. It happened even though the west face was in tension because the main-bars in the west face were significantly stretched during the load cycle to $12\delta_y$ eastwards, and buckled while the column was returning to the centre point.

In the latter half of the fourth loading cycle to

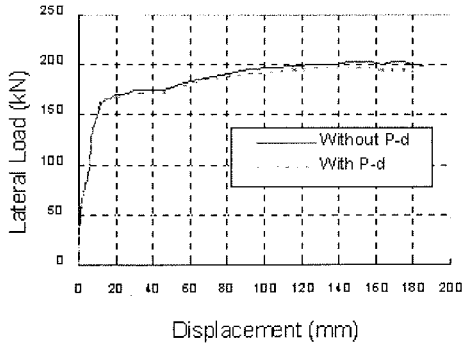

Fig.12 Lateral load-Displacement Relationship for Specimens-1 and 2 determined from Moment-Curvature Analysis

Table 5 Theoretical Ideal Lateral Strength of Test Specimens

Specimen No.	Ideal Lateral Strength L_n (kN)			
	Moment-Curvature analysis		NZ3101	
	Without P-δ	With P-δ	Without P-δ	With P-δ
1	169.5	168.7	170.0	169.0
2	169.5	168.7	170.0	169.0
3	168.5	167.8	168.4	167.5
4	169.2	168.4	169.5	168.5
5	158.0	157.2	152.8	152.2

$-10\delta_y$ westwards, some cracks on a main-bar at the south-east corner were observed on the inside surface of the bar at a buckled part, when it was extended in tension.

Until the test was terminated after two cycles to $\pm 2\delta_y$, the cover concrete continued spalling off gradually but no main-bar was broken although some cracks were detected on the main-bars at the corners.

c) Specimen-3

The measured displacement to the north corresponding to the three quarters of the calculated ultimate load was about 90% larger and the average of other three displacements was 30% larger than that of Specimens-1, 2 and 3. It was found that this difference was caused by a small extra rotation of the counter-weight basket on which the measuring frame was fixed, due to lack of high strength plaster applied between the counter-weight frame and the base block. This error is adjusted for the analysis. The first buckling of the main-bars was detected on the east face during the first cycle to $6\delta_y$ in the east-west direction.

A significant drop of lateral load was detected on the hysteresis loop in the south-north loading to $6\delta_y$. During the first cycle to $8\delta_y$ in the north-south direction, some main-bars failed. This was regarded as the end of the test.

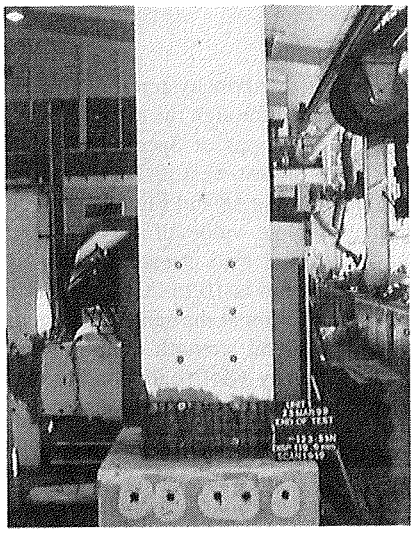

Fig.13 Specimen-1 After Test (East Face)

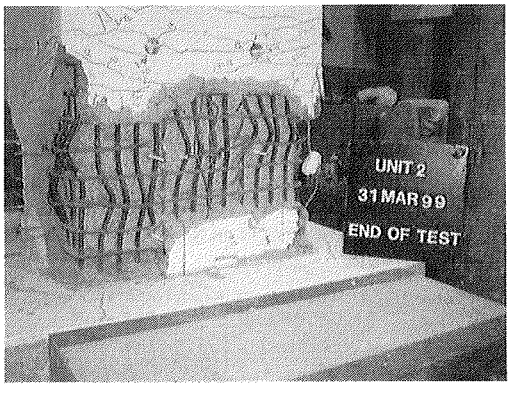

Fig.14 Specimen-2 After Test (From North-East)

d) Specimen-4

During the first cycle to $6\delta_y$, the first buckling of main-bars occurred only at the south-east corner while this corner was in compression. All the main-bars buckled during the second cycle to $6\delta_y$. The test was abandoned at the end of the second cycle to $8\delta_y$, because of the significant drop of the lateral load resistance of the column.

e) Specimen-5

After the loading cycle to three-quarters of the ideal strength of the column, the number of cracks was found to be much greater than that of Specimen-1 at the same stage due to the much weaker concrete. The first buckling of main-bars occurred on the east face in the first cycle to $6\delta_y$(east). Some main-bars failed during the second cycle to $10\delta_y$, and the test was then terminated because of the significant drop off of the lateral load resistance of the column.

4.TEST RESULTS

(1) Hysteresis loops

Fig.16 to **Fig.20** show hysteresis loops of all the specimens obtained through the tests.

The hysteresis loops of Specimens-3 and 4 are shown for each of east-west and south-north directions separately in **Fig.18** and **Fig.19**. As seen in the figures, the absolute value of the maximum and minimum horizontal load at each loading cycle in south-north direction is 10 to 20 % smaller than in the east-west direction at the same loading stage. It shows that the lateral strength of the column was obviously affected by a horizontal loading applied in another direction, as reported by Mashiko et al.[7].

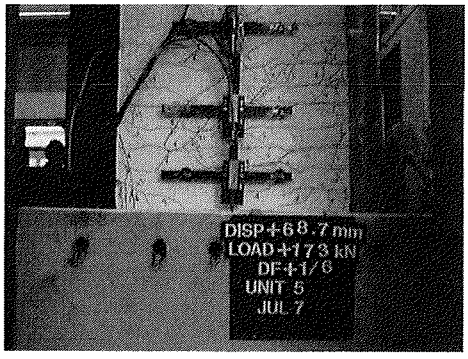

Fig.15 Significant Shear Cracks on North Face (Specimen-5)

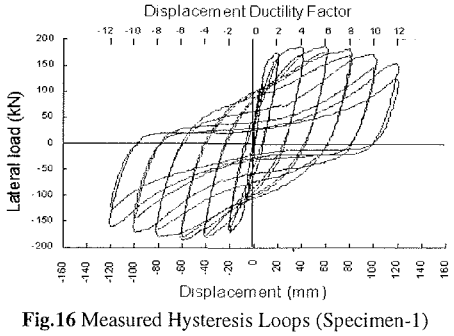

Fig.16 Measured Hysteresis Loops (Specimen-1)

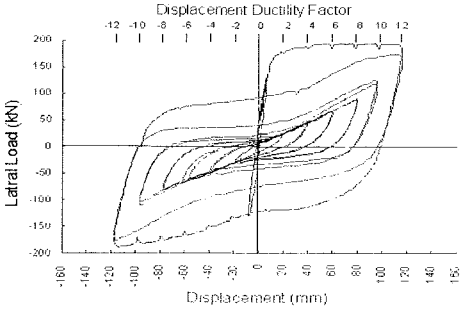

Fig.17 Measured Hysteresis Loops (Specimen-2)

(2) Plastic hinge zone length

a) Calculation of plastic hinge zone length

Paulay & Priestley [15] recommended that the plastic hinge zone length L_p of a rectangular reinforced concrete column is calculated as

$$L_p = 0.08\,h + 0.022\,d_b f_y \qquad (6)$$

where, h is the column height; d_b is the diameter of the vertical main-bars; and f_y is the yield strength of the vertical main-bars. The second part of Eq(6) is for the additional deflection of the column due to the yield penetration of the vertical main-bars at the base

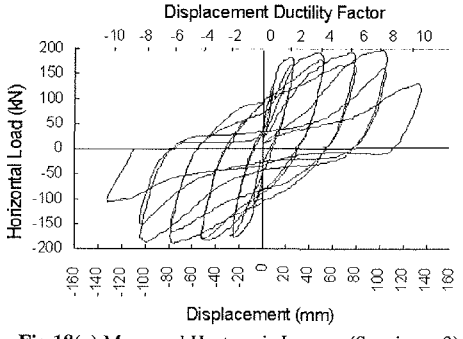

Fig.18(a) Measured Hysteresis Loops (Specimen-3): In East-West Direction

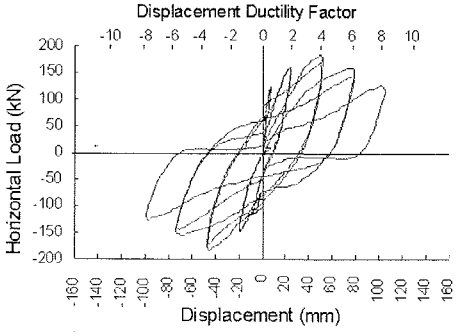

Fig.18(b) Measured Hysteresis Loops (Specimen-3) : In North-South Direction

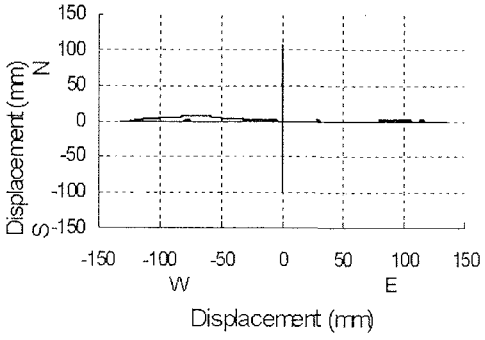

Fig.18(c) Measured Hysteresis Loops (Specimen-3): Loading Orbit

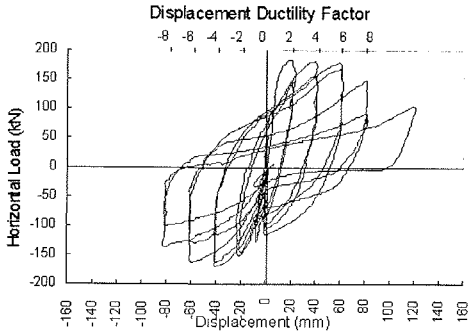

Fig.19(a) Measured Hysteresis Loops (Specimen-4) : In North-South Direction

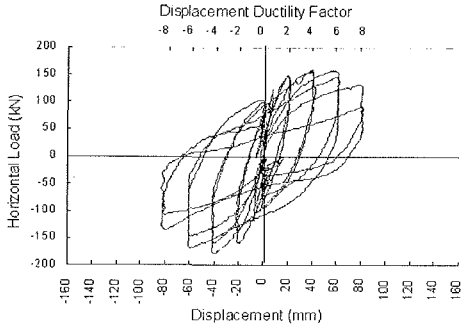

Fig.19(b) Measured Hysteresis Loops (Specimen-4): In East-West Direction

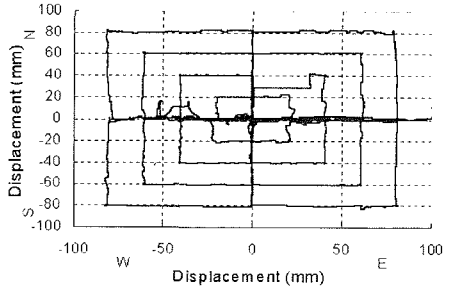

Fig.19(c) Measured Hysteresis Loops (Specimen-4): Loading Orbit

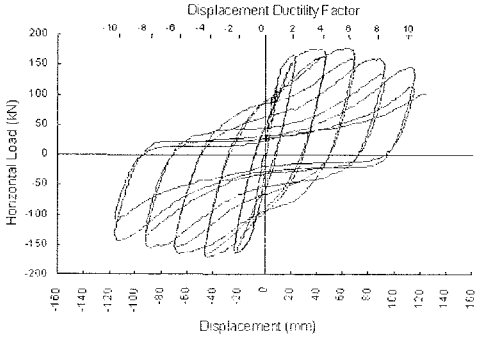

Fig.20 Measured Hysteresis Loops (Specimen-5)

of the column. The total deflection of the column due to flexure, δ, at the height h is calculated using Eq(7) (Park & Paulay [16]).

$$\delta = \delta_y + \delta_p = \phi_y h^2 / 3 + \phi_p L_p (h - L_p / 2) \quad (7)$$

where, δ_y is the yield displacement of the column, δ_p is the plastic displacement of the column, ϕ_y is yield curvature at the base of the column and ϕ_p is plastic curvature in the plastic hinge zone. In application of Eq(7) to the test results, δ is the measured displacement at the loading point and δ_y is calculated as described in §2.(1) during the tests, then δ_p and ϕ_y are obtained as

$$\delta_p = \delta - \delta_y \quad (8)$$

$$\phi_y = 3\delta_y / h^2 \quad (9)$$

where $h = 2250$ mm

ϕ_p is obtained from the curvature at the base of the column ϕ and ϕ_y as Eq(10). Here, ϕ is substituted by the average curvature between the base of the column and the bottom most potentiometer, calculated using Eq(2).

$$\phi_p = \phi - \phi_y \quad (10)$$

L_p is obtained using Eq(11) derived from Eq(7).

$$L_p = \frac{\phi_p h - \sqrt{(\phi_p h)^2 - 2\phi_p \delta_p}}{\phi_p} \quad (11)$$

When the displacement of the column is calculated using Eq(7), the effect of the yield penetration of the main-bars is considered in L_p, as mentioned above. On the other hand, the experimental value of ϕ used in Eq(10) also contains the additional curvature due to the yield penetration of the main-bars as does ϕ_p obtained from ϕ. Therefore, L_p is underestimated by Eq(11) if ϕ_p from Eq(10) is used in Eq(11) without eliminating the effect of the yield penetration from ϕ_p.

Figs.21 to **25** show the curvature distribution along the five columns to displacement ductilities of 6 except for Specimen-2 when curvatures were measured to μ_Δ=12. The maximum curvature is always close to the base of the column even though the major damage of the column seemed to be between 100 to 200mm above the base. This larger curvature at the base of the column is caused by the wide crack seen at the base of the columns (see

Fig.26). It is assumed that this crack was formed because of the construction joint and the maximum bending moment acting at the base of the column; this crack is associated with the yield penetration of the vertical main-bars. Because the bottom end of main-bars is well anchored at the bottom of the base block with 90 degree hooks, no pull-out of main-bars, only except yield penetration, is to be assumed. The curvatures shown in **Fig.21** to **Fig.25** are only for smaller values of μ_Δ except that of Specimen-2 because in the later stage of the tests the cover concrete bulged due to the buckling of main-bars and affected the potentiometers which measured the curvature.

The theoretical value of L_p suggested by Paulay & Priestley [15] is calculated using Eq(6) with h=2250mm, d_b=10mm and f_y =306MPa as

$$L_p = 0.08 \times 2250 + 0.022 \times 10 \times 306$$
$$= 180 + 67$$
$$= 247 \text{ (mm)} \qquad (12)$$

where the influence of the yield penetration of the main-bars is 67mm. The percentage of plastic displacement of the column resulting from yield penetration is obtained as follows using Eq(7).

without yield penetration :

$\delta_p = \phi_p \, 180 \, (2250 - 180 / 2) = 388{,}800 \, \phi_p$

with yield penetration :

$\delta_p = \phi_p \, 247 \, (2250 - 247 / 2) = 525{,}246 \, \phi_p$

therefore, the influence of yield penetration is

$(525{,}246 - 388{,}800) / 525{,}246 \times 100 = 26 \, \%$

This percentage is constant in Eq(6) and the plastic displacement is in proportion to the plastic curvature according to Eq(7). Therefore, the percentage effect of the yield penetration on the measured maximum curvature can also be assumed to be 26%, and hence the measured maximum curvature was reduced by 26% before L_p was calculated using Eq(7). **Fig.27** to **Fig.31** show the relationships between the calculated plastic hinge zone length L_p and the displacement ductility factor μ_Δ with the theoretical values of the plastic hinge zone length. The theoretical value by Paulay & Priestley [15] is 247mm as seen in Eq(9) and that for the Japanese specification is 275mm obtained using Eq(13).

$$L_p = 0.2h - 0.1D \quad (0.1D \le L_p \le 0.5D) \qquad (13)$$

Where, h is the height from the base of the column to the superstructure mass and D is the lateral width of the column.

The maximum plastic curvature calculated for the first cycle of a given displacement is used. The values of L_p for Specimen-2 in **Fig.28**, were calculated only by the data obtained in the second cycle of loading from zero to $\pm 12\delta_y$. In **Fig.29**, μ_Δ for Specimen-3 was adjusted for the extra rotation mentioned in §3.(3).c)

b) Comparison between experimental and theoretical value of L_p

The findings from **Fig.27** to **Fig.31** are,

1) The plastic hinge zone length L_p increases as the displacement δ increases during monotonic loading (**Fig.28**).

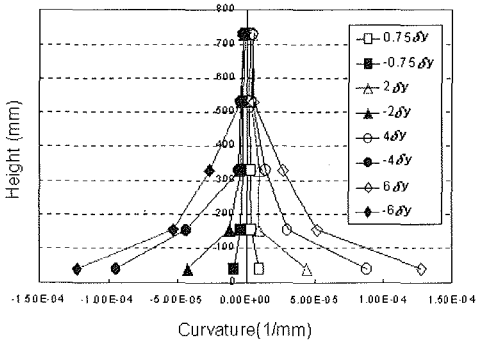

Fig.21 Curvature Distribution of Specimen-1

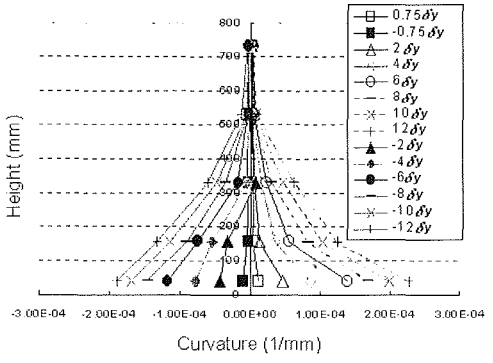

Fig.22 Curvature Distribution of Specimen-2

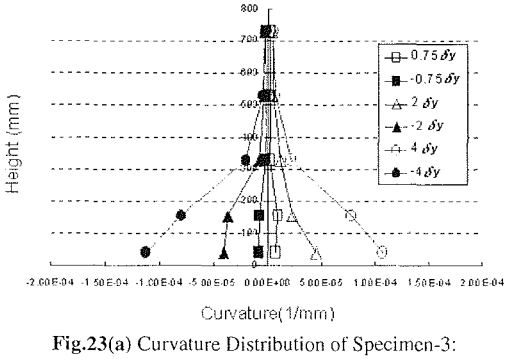

Fig.23(a) Curvature Distribution of Specimen-3: East-West Direction

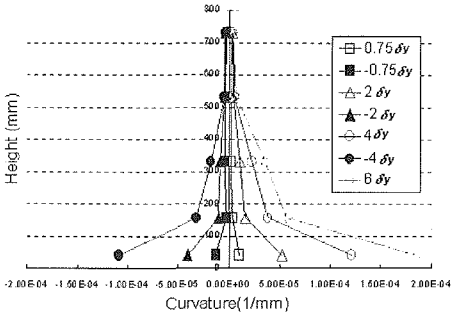

Fig.23(b) Curvature Distribution of Specimen-3: North-South Direction

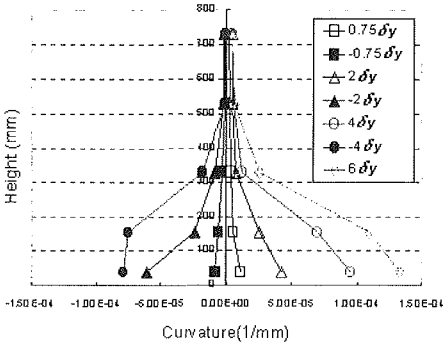

Fig.24(a) Curvature Distribution of Specimen-4: East-West Direction

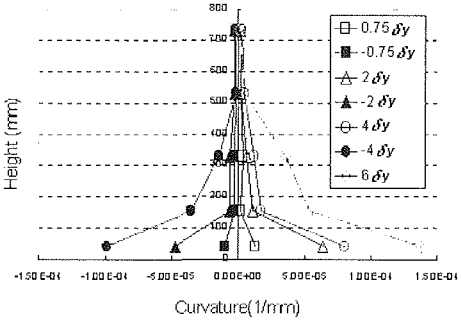

Fig.24(b) Curvature Distribution of Specimen-4: North-South Direction

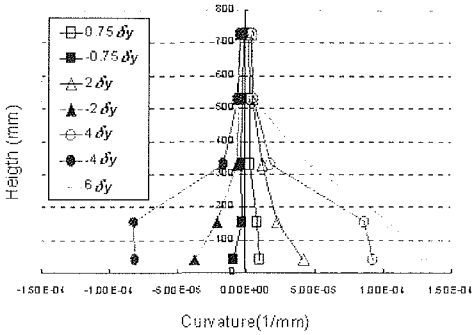

Fig.25 Curvature Distribution of Specimen-5

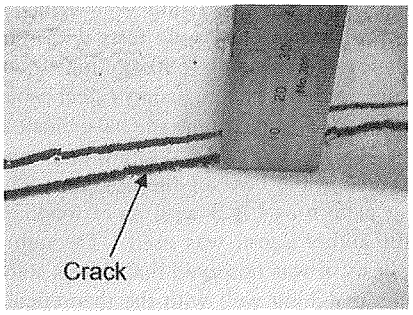

Fig.26 Example of Wide Crack at the Base of Column (Specimen-2, at $4\delta_y$ to east)

2) L_p tends to be stable at around the theoretical values after some cyclic loading (**Fig.27** to **Fig.31**, except **Fig.28**).
3) No significant difference is observed between **Fig.27**, **Fig.29** and **Fig.30** except L_p for μ_Δ=2. This means that L_p is not affected by bi-directional loading after some cycles of loading.
4) From 2) and 3), it can be assumed that extra cycles of bi-directional loading stabilise the value of L_p.
5) Theoretical values of the plastic hinge zone length overestimate that for small displacement ductility factor (say, when μ_Δ=2). Otherwise, experimental values correspond well with the theoretical values for $\mu_\Delta \geq 6$.
6) All the values of L_p for Specimen-5 are larger than the corresponding values for Specimen-1. This means that the concrete strength f'_c could affect L_p even though it is not included in the equations for L_p in both Paulay & Priestley [15] and the Japanese specification [8].

c) Details of yield penetration

Shima et al. [17] defined a formula to obtain the extracted (pull-out) length of a main-bar from the base block, S_y, due to the yield penetration, as Eq(14).

$$S_y = \alpha S_{yl} \tag{14}$$

Where $$S_{yl} = \frac{7.4\varepsilon_y (6 + 3500\varepsilon_y) d_b}{f'^{2/3}_c} \tag{15}$$

$$\alpha = 1 + 0.9e^{0.45(1-a/d_b)} \tag{16}$$

α is a factor to consider the effect of centre-to-centre distance a (mm) of the main-bars; S_{yl} is the extracted length of a single main-bar (mm); ε_y is the yield strain; d_b is the diameter (mm) of the vertical main-bars; and f'_c is the specified compressive strength of the concrete (MPa). S_y is assumed to be stable regardless of the strain in the main-bar after

yielding. Ogasawara & Tsuno [18),19)] actually measured S_y in a series of seismic tests with reinforced concrete bridge columns (650×650mm square section) subjected to a flexure, using a steel cable which was set in a pipe penetrating the base block and one end of the cable was attached to a main-bar (d_b=10mm) at the base of the column. The same loading pattern as **Fig.3** with more loading cycles than the author's test, was used. Through Ogasawara's tests, it was observed that S_y was stable after yielding, matching well with the theoretical values

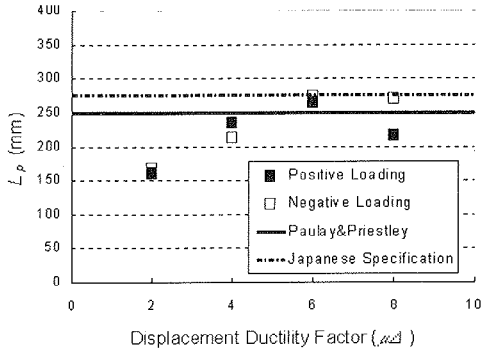

Fig.27 Plastic Hinge Zone Length-Displacement Ductility Factor Relationship for Specimen-1

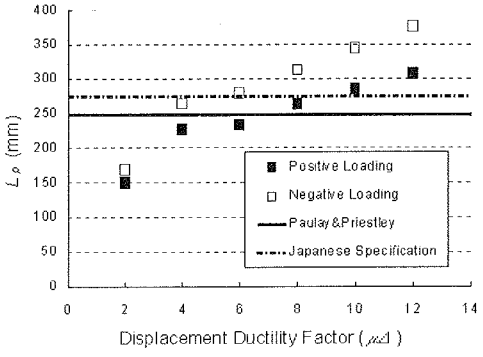

Fig.28 Plastic Hinge Zone Length-Displacement Ductility Factor Relationship for Specimen-2

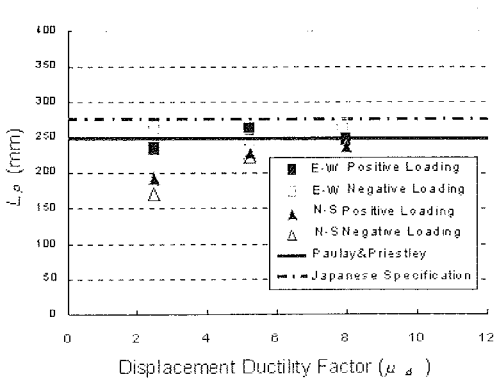

Fig.29 Plastic Hinge Zone Length-Displacement Ductility Factor Relationship for Specimen-3

using Eq(14) to Eq(16) inclusive, and then stepped up when the strain of the main-bar reached about 0.02 in the cycle of loading to $1\delta_y$. It was also observed that the percentage of displacement (not plastic displacement) of the column resulting from yield penetration into the column base was stable at from 10 to 15% all through their tests which finished at about $6\delta_y$. These observations support Eq(14) to Eq(16) by Shima et al. at the early stage of the tests, and also support Eq(6) by Paulay & Priestley [15)] concerning the stable influence of yield penetration on the displacement of the column.

From these findings, it is assumed that S_y is stable at a low level after the main-bars yield, and at some stage, it increases to some higher level which is in proportion to the displacement of the column. From the observation of **Fig.27** to **Fig.31**, it is also assumed that the "step point" of S_y is affected by the number of the cycles of loading. **Fig.32** and **Fig.33** show the strain history of the main-bars at 50mm below the base of the column (50mm deep in the base block), for Specimen-1 and Specimen-4. The strain steps up during the loading cycles to $4\delta_y$ in Specimen-1 with uni-axial loading, on the other hand, the strain steps up at the early stage of the loading cycles to $2\delta_y$ in Specimen-4. It corresponds well to the assumptions made above.

S_y of Specimen-1 for the early stage is calculated by the Shima's method using Eq(14) to Eq(16), inclusive, and the numbers; d_b =10mm, ε_y =0.0015, f'_c =30MPa and a = 38mm, as

$$S_{y1} = 7.4 \times 0.0015\ (6+3500\times0.0015)\ 10 / 30 = 0.130 \text{ mm}$$

$$\alpha = 1+0.9\ e^{(1-38/10)} = 1.055$$

therefore, $S_y = 0.130 \times 1.055 = 0.137$ mm

With this value of S_y and assuming the distance between the main-bars with S_y from the neutral axis of the section at the base of the column is 440mm (from Moment-Curvature analysis, at μ_Δ =2), the rotation of the column due to the yield penetration, θ_{yp}, is

$$\theta_{yp} = 0.137 / 440 = 0.000311$$

Therefore, the displacement of the column due to the yield penetration, δ_{yp}, is obtained as

$$\delta_{yp} = \theta_{yp}\ h = 0.000311 \times 2250 = 0.7 \text{ mm}$$

This value is only 7.1% of 9.9mm which is the plastic displacement of Specimen-1 corresponding to μ_Δ =2, and less than one-third of 26 % derived using Eq(7). It means, supposing the behaviour of yield penetration follows Shima's equations at the

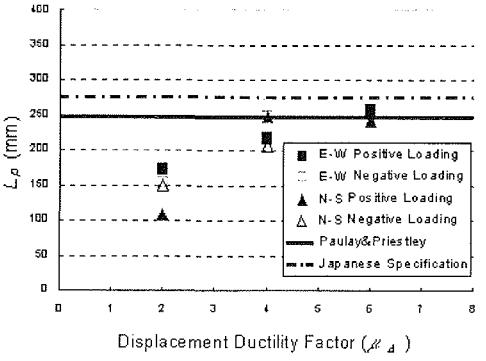

Fig.30 Plastic Hinge Zone Length-Displacement Ductility Factor Relationship for Specimen-4

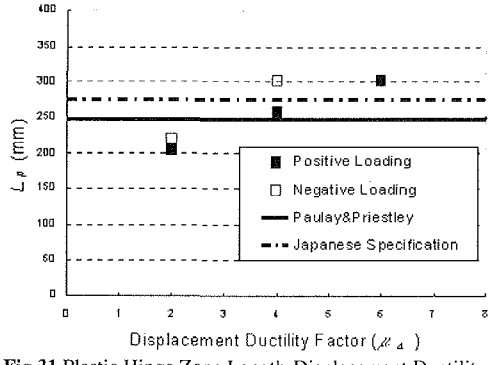

Fig.31 Plastic Hinge Zone Length-Displacement Ductility Factor Relationship for Specimen-5

early stage, actual L_p is smaller than that shown in **Fig.27** to **Fig.31**, which is based on the influence of 26%.

d) Obtained plastic hinge length in tests

Only the values of L_p corresponding to μ_Δ =2 (μ_Δ =2.74 for Specimen-3) are recalculated with the influence of 7.1%, and shown in **Fig.34** with other values of L_p for μ_Δ larger than 4. Each L_p is the average of all values at the same μ_Δ, for each specimen. A revised L_p-μ_Δ relationship is shown in **Fig.34**, which consists of two parts; a horizontal line at the theoretical L_p calculated using Eq(6) or Eq(13) for μ_Δ more than 4, and a line connecting a point with a quarter of the theoretical L_p at μ_Δ =1 with the horizontal line at μ_Δ =4.

If the plastic hinge zone length is overestimated in the design of a reinforced concrete column, the displacement of the column for a given plastic curvature will be greater, leading to a smaller design seismicity. **Fig.34** shows that the obtained L_p for μ_Δ less than four was smaller than the theoretical values. This small L_p, however, was formed before the column was seriously damaged because the specimens were designed for much larger displacement ductility factor.

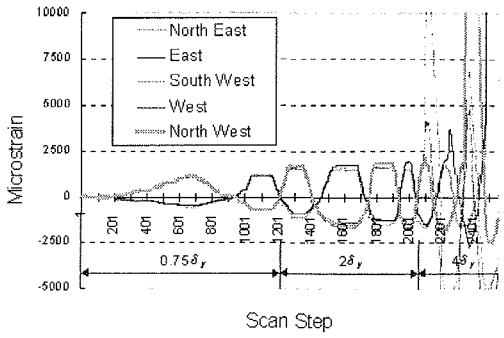

Fig.32 Strain History of Main-bars 50mm below the Base (Specimen-1)

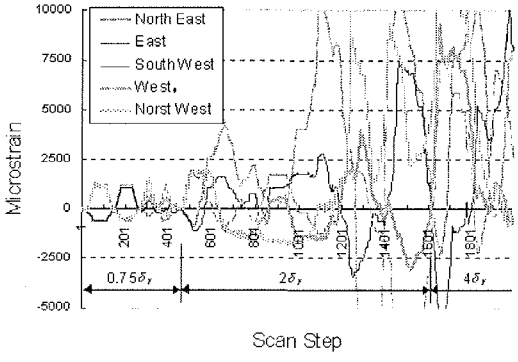

Fig.33 Strain History of Main-bars 50mm below the Base (Specimen-4)

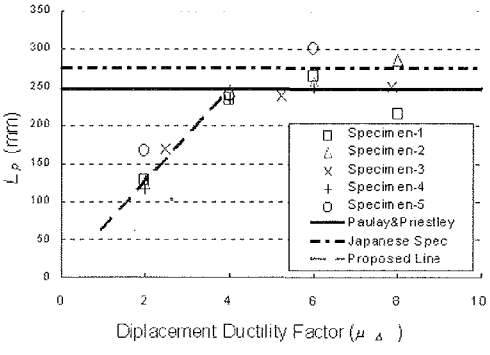

Fig.34 Plastic Hinge Zone Length Obtained in Tests

Some more experimental study is needed in order to clearly see whether the smaller theoretical values for L_p should be used in the design of a column with small displacement ductility factor capacity.

(3) Energy dissipation

a) Calculation of dissipated energy

The energy dissipated by a test specimen is defined as the area enclosed by the hysteresis loop of the lateral load-displacement relationship in both of the positive and negative side, with units of kN·mm. The calculation is carried out by a spreadsheet, nu-

merically adding up the area in a loop for each completed loading cycle, up to the cycle before the specimen reached the ultimate state. For Specimen-3, the measured displacement was adjusted by subtracting the difference between the measured yield displacement of Specimen-3 and the average yield displacement of Specimens-1, 2 and 4, in order to eliminate the effect of the extra rotation of the measuring frame, explained in §3.(3).c).

b) Individual cycle energy

Fig.35 to **Fig.39** show the dissipated energy by each individual loading cycle and the accumulation of the dissipated energy. In **Fig.37** for Specimen-3, one column in the graph is the energy dissipated by two loading cycles to a given displacement in the same direction. In **Fig.38** for Specimen-4, one column is for half of a completed double-8 shaped loading cycle (one 8 shape), seen in **Fig.7(c)**.

The second loading cycle to the same displacement always dissipates less energy than the first cycle due to the damage caused by the former cycle, as seen in all **Fig.35** to **Fig.39**. A significant drop of energy dissipation is observed after the buckling of main-bars and the failure of transverse reinforcement. The allowable ductility factor of the prototype column for the Type-2 earthquake is 6. All of Specimens-1, 3 and 4 (even 5) sustained a good energy dissipation until at least the loading cycles to $6\delta_y$ were completed, even though the bi-directional loading for Specimens-3 and 4 caused early buckling of the main-bars and the failure of transverse reinforcement.

Buckling of the main-bars and failure of transverse reinforcement in Specimen-2 occurred in the first cycle to $12\delta_y$ eastwards and it caused a significant drop of energy dissipation from the following loading cycle, as seen in **Fig.36**. This drop is also observed in **Fig.17**. For the loading cycles to lower displacements, the loading loops are pinched due to the low lateral strength and do not dissipate as much energy as that for the other test specimens with the same displacement.

c) Total dissipated energy

Fig.40 shows the comparison of the total dissipated energy until the ultimate state defined in §2.b) is reached, for all the test specimens.

The total dissipated energy of Specimens-1, 3 and 4 are approximately the same, meaning that the bi-axial load did not affect the total energy dissipation capacity of a column until the ultimate state. This finding agrees with the conclusion stated by Ohno & Nishioka [20] that the total dissipated energy by a column is independent of the loading sequence.

Specimen-2 dissipated much less energy than Specimens-1, 3 and 4, but the ultimate state defined by Zahn et al. [10] can not be applied in this case be-

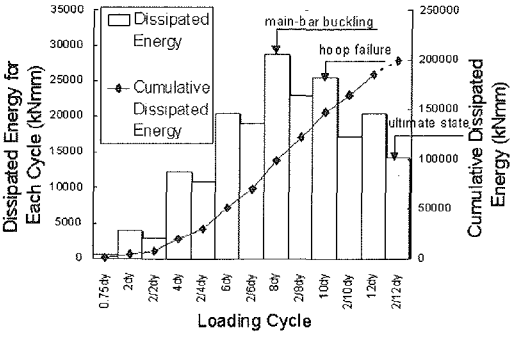

Fig.35 Individual Cycle Energy (Specimen-1)

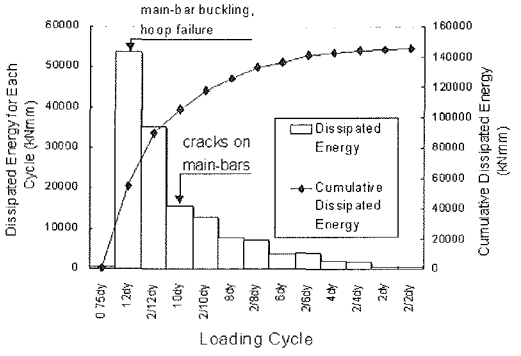

Fig.36 Individual Cycle Energy (Specimen-2)

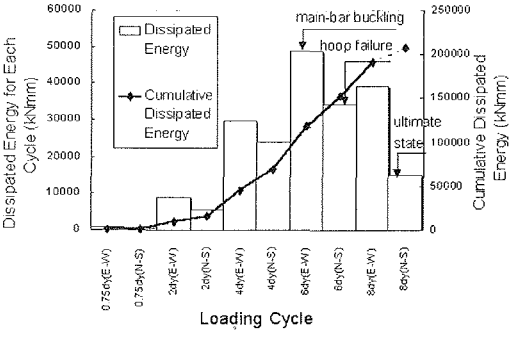

Fig.37 Individual Cycle Energy (Specimen-3)

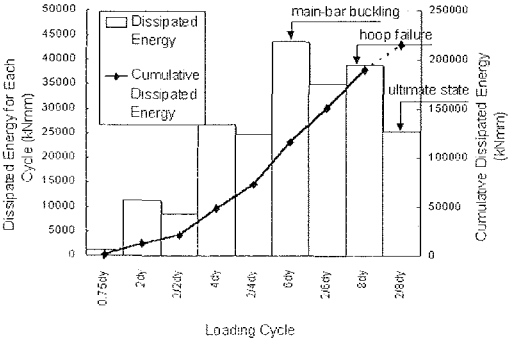

Fig.38 Individual Cycle Energy (Specimen-4)

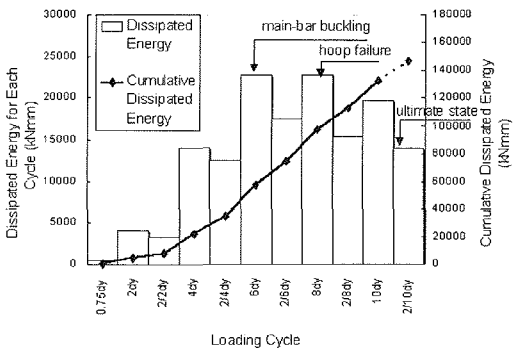

Fig.39 Individual Cycle Energy (Specimen-5)

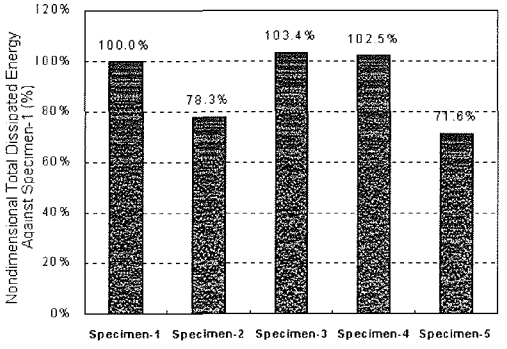

Fig.40 Total Dissipated Energy

cause the loading pattern was opposite to that for Specimen-1. When the first cycle to $10\delta_y$ was completed on Specimen-2, however, some cracks were found on the main-bars showing a significant damage on the column. Therefore, no more significant energy dissipation capacity is expected, and the total dissipated energy shown in **Fig.40** could be recognised as the capacity of Specimen-2. This means that the loading pattern applied to Specimen-2 affected the total energy dissipation capacity of the column, causing the buckling of main-bars and the failure of transverse reinforcement, and decreasing the shear strength at the base of the column, at an early stage of the test.

The dissipated energy by Specimen-5 is the lowest among all the five test specimens. Even though the ideal lateral strength of the specimen was estimated as 90% of that of Specimen-1 as seen in **Table 2**, energy dissipation capacity was only 71.6% of Specimen-1. It shows that the effect of concrete strength on the energy dissipation capacity of the column is more significant than its effect on the ideal strength of the column.

5. CONCLUSIONS

1) The plastic hinge zone length L_p tends to be stable at around the theoretical values after some cyclic loadings and is not affected by bi-directional loading. The plastic hinge zone length is shorter than the theoretical values until the displacement ductility factor μ_Δ reaches about 4. The concrete strength of a column might affect the plastic hinge zone length L_p.
2) If an extremely large displacement, such as μ_Δ=12, for the specimens used in this research, is applied to a column at the early stage of a cyclic loading, it may lead to the buckling of the main-bars and confinement failure with only small energy dissipation. However, as long as the displacement amplitude in the cyclic loading starts at a small level and increases step-by-step, like the standard loading pattern suggested by Park [9], the energy dissipation capacity of a column until the ultimate state is the same for both uni-directional and bi-directional loading.
3) The maximum displacement of a column when it reaches the ultimate state in a bi-directional cyclic loading, is smaller than that of the same column subjected to the standard uni-directional loading pattern suggested by Park [9]. However, the design available displacement ductility factor was met because of a safety factor defined in the Japanese specification.

REFERENCES

1) Kawashima, K. and Koyama, T.: Effect of Number of Loading Cycles on Dynamic Characteristics of Reinforced Concrete Bridge Pier Columns, *Proceedings of JSCE*, No.392/I-9, pp.205-213, April, 1988.
2) Ozaka, Y., Suzuki, M. and Kanie, H.: Effect of Loading Rate and Loading Pattern on Behaviours of Reinforced Concrete Columns (in Japanese), *Structural Engineering Journal*, JSCE, Vol.34A, pp.911-922, April, 1988.
3) Takemura, H. and Kawashima, K.: Effect of Hysteresis on Ductility Capacity of Reinforced Concrete Bridge Piers (in Japanese), *Structural Engineering Journal*, JSCE, Vol.43A, pp.849-848, March, 1997.
4) Hoshikuma, J., Unjo, S., Kawashima, K. and Nagaya, K.: A Ductility Evaluation of Reinforced Concrete Columns Based on Loading History and Plastic Curvature (in Japanese), *Structural Engineering Journal*, JSCE, Vol.44A, pp.877-888, March, 1998.
5) Miyaji, K., Nakazawa, N., Kawashima, K. and Watanabe, M.: Ductility Capacity of Reinforced Concrete Bridge Columns using High Strength Concrete and High Strength Reinforcement (in Japanese), *Proceedings of the 6th Symposium on Ductility Design Method for Bridges*, pp.75-81, January, 2003.
6) Sato, Y., Yoshimura, M. and Tsumura, K.: Deformation Characteristics of Reinforced Concrete Column Loaded in Two Horizontal Directions, *Concrete Engineering Journal*, Vol.16, No.2, [2108], 1994.
7) Mashiko, N., Mutsuyoshi, H., Tanzo, W. and Machida, A.: Elasto-Plastic Behaviour of Reinforced Concrete Bridge

Column Seismically Loaded in Two Horizontal Directions, *Concrete Engineering Journal*, Vol.16, No.2, [2212], 1994.
8) Japan Road Association: *Guide Specification of Seismic Design of Highway Bridges* (in Japanese), 1996.
9) Park, R.: Evaluation of Ductility of Structures and Structural Assemblages from laboratory Testing, *Bulletin of the New Zealand National Society for Earthquake Engineering*, Vol.22, No.3, September, 1989.
10) Zahn, F.A., Park, R. and Priestley, M.J.N.: Design of Reinforced Concrete Bridge Columns for Strength and Ductility, Department of Civil Engineering, University of Canterbury, New Zealand, March, 1986.
11) Japan Road Association: *Seismic Design Data for Highway Bridges* (in Japanese), 1997.
12) *NZS 3101, Concrete Structures Standard, Part-1:The Design of Concrete Structures*, Standards New Zealand, Wellington, 1995.
13) Sato, Y., Tanaka, H. and Park, R.: Reinforced Concrete Columns with Mixed Grade Longitudinal Reinforcement, Department of Civil Engineering, University of Canterbury, August, 1993.
14) Mander, J.B., Priestley, M.J.N. and Park, R.: Seismic Design of Bridge Piers, Department of Civil Engineering, University of Canterbury, August, 1984.
15) Paulay, T. and Priestley, M.J.N.: *Seismic Design of Reinforced Concrete and Masonry Buildings*, John Wiley and Sons, New York, 1992.
16) Park, R. and Paulay, T.: *Reinforced Concrete Structures*, John Wiley, New York, 1975.
17) Shima, H., Syu, L. and Okamura, H.: Bond-Slip-Strain Relationship of Deformed Bars Embedded in Massive Concrete (in Japanese), *Proceedings of JSCE*, No.378, Japan Society of Civil Engineers, Tokyo, February, 1987.
18) Ogasawara, M. and Tsuno, K.: An Experimental Study Concerning Tie-bars of Reinforced Concrete Piers, *Proceedings of 9th REAAA Conference held in Wellington, New Zealand*, 1998.
19) Metropolitan Expressway Public Corporation: Research Report concerning Highway Bridges (in Japanese), Concrete Structure Group, 1996.
20) Ohno, T. and Nshioka, T.: An Experimental Study on Energy Absorption Capacity of Columns in Reinforced Concrete Structures, *Structural Engineering/Earthquake Engineering, Proceedings of the Japan Society of Civil Engineers*, Vol.1, No.2, October, 1984.

(Received February 17, 2003)